RESEARCH ARTICLE

JOR Spine OPEN ACCESS

Clinical efficacy and biomechanical analysis of a novel hollow pedicle screw combined with kyphoplasty for the treatment of Kümmell disease

Shixiao Zhong[1,2] | Hui Zhong[2,3] | Kun Huang[2,3] | Yayu Zhao[1,2] | Wen Lei[1,2] | Weichao Li[1,2,3]

[1]Faculty of Medical Science, Kunming University of Science and Technology, Kunming, China

[2]Department of Orthopaedics, The First People's Hospital of Yunnan Province, Affiliated Hospital of Kunming University of Science and Technology, Kunming, China

[3]Yunnan Key Laboratory of Digital Orthopaedics, Affiliated Hospital of Kunming University of Science and Technology, Kunming, China

Correspondence
Weichao Li, Department of Orthopaedics, The First People's Hospital of Yunnan Province, Affiliated Hospital of Kunming University of Science and Technology, No. 157, Jinbi Road, Kunming, 650032, China.
Email: liweichao0394@sina.com

Abstract

Background: Vertebral augmentation is the preferred treatment for Kümmell disease (KD), but there exists a risk of cement displacement resulting in severe back pain and exacerbation of kyphosis. The study aimed to investigate the efficacy and safety of a novel hollow pedicle screw combined with kyphoplasty (HPS-KP) for treating KD, effectively preventing postoperative bone cement displacement.

Methods: The prospective study included 50 KD patients with no neurological deficit detected during clinical and radiological evaluation who underwent HPS-KP ($n = 25$) and PKP ($n = 25$) surgeries. The visual analogue scale (VAS) score, Oswestry dysfunction index (ODI), anterior vertebral height (AVH), wedge-shape affected vertebral Cobb angle (WCA), bisegmental Cobb angle (BCA), and complications were evaluated and compared in both groups. Besides, a finite element (FE) model of T11-L2 was constructed. The stress distributions, maximum von Mises stresses of vertebrae and bone cement, and maximum displacement of bone cement were compared and analyzed.

Results: The VAS and ODI scores at 3 days, 3 and 6 months, and 1 year after surgery significantly improved in both groups ($p < 0.05$). The AVH, BCA, and WCA significantly improved initially after the surgery in both groups ($p < 0.05$). The displacement of M2 was larger than other models, especially in flexion, right bending, and left and right rotation, while that of M6 was the lowest under all conditions.

Conclusion: HPS-KP was a safe and effective treatment for KD, effectively relieving pain, restoring vertebral height, and correcting local kyphosis, and it had better

---

Shixiao Zhong and Hui Zhong contributed equally to this study.

biomechanical stability and safety than ordinary single PKP and PKP combined with pediculoplasty in avoiding cement loosening and displacement.

1 | INTRODUCTION

Kümmell disease (KD) was first proposed by Dr. Hermann kümmell in 1891 as a clinical phenomenon of delayed post-traumatic vertebral collapse,[1] causing acute or chronic low back pain and local kyphosis deformity, which seriously affects the quality of life of patients.[2] The phenomenon of intravertebral vacuum cleft (IVC) was deemed as the representative imaging sign of avascular osteonecrosis of the vertebral body, and the IVC was mostly located at the center of the vertebra or the side close to the vertebral endplate.[3] According to imaging evaluation, KD was divided into three stages: Stage I, vertebral compression rate <20% with IVC sign; Stage II, vertebral compression rate >20% with dynamic mobile fracture and adjacent disc degenerative disease; and Stage III: posterior cortex breakage of vertebral body with cord compression.[4] At present, although percutaneous kyphoplasty (PKP) and percutaneous vertebroplasty (PVP) are unanimously regarded as effective and the preferred treatments for KD (stages I and II), providing immediate pain relief and improving the quality of life of patients.[5,6] However, both procedures mainly utilize polymethylmethacrylate (PMMA) bone cement as the material. Due to its lack of osseointegration ability, it is prone to loosening and displacement, requiring further surgical intervention.[7–9]

A retrospective study found that the incidence of cement displacement was 18.20%, and the time of post-operative cement displacement ranged from 1.8 to 38.2 months.[10] It has been reported that the occurrence of bone cement displacement can lead to serious complications, such as progressive severe back pain, spinal instability, delayed paraplegia, and neurological decline.[11–15] To prevent the occurrence of bone cement displacement, there are reports in the literature trying to improve the way of bone cement injection or use the pedicle screw internal fixator, such as the vertebroplasty combined with pediculoplasty,[13] the Re-BKP method,[16] the insertion of hollow pedicle screws into the cement block,[17] and the use of bone cement screw fixation.[18] However, these reported treatments are far from perfect, and issues such as inadequate cement fixation or imperfect internal fixation screws design persist.

This study aims to (1) propose a modified surgical procedure with a novel pedicle screw for the treatment of KD; (2) compare the differences between PKP and HPS-KP (A novel hollow pedicle screw combined with kyphoplasty); and (3) explore the causes of bone cement displacement and effective solutions.

2 | MATERIALS AND METHODS

2.1 | Study design

Ethical approval for this study was obtained from the First People's Hospital of Yunnan Province (No. KHLL2021-KY085). This prospective nonrandom case–control study collected data on KD patients treated with HPS-KP and PKP at our center between January 1, 2020 and June 31, 2023. All patients satisfied the following inclusion criteria: (1) the patients were diagnosed with KD without neurological impairment symptoms; (2) delayed vertebral compression and IVC presence were identified based on CT and MRI imaging; (3) KD patients received unilateral or bilateral HPS-KP and PKP surgery, and the minimum follow-up time was 6 months; and (4) patients with osteoporosis were diagnosed according to national osteoporotic fracture guidelines.[19] The exclusion criteria: (1) patients with primary and secondary spinal tumors or spinal tuberculosis and (2) patients with serious surgical contraindications, such as cardiovascular and cerebrovascular disorders, including unstable angina pectoris, severe heart failure, severe arrhythmia, acute cerebral infarction, cerebral hemorrhage, and other life-threatening conditions.

A total of 50 patients were enrolled in this study, comprising 25 individuals (8 males and 17 females; mean age 73.00 [68.50, 79.00] years) treated with HPS-KP and 25 participants (5 males and 20 females; mean age 70.00 [67.00, 75.50] years) treated with PKP. The specific follow-up scheme is shown in Figure 1. According to Li's[4] classification, the HPS-KP group consisted of 3 cases of stage I, 11 cases of stage II, and 11 cases of stage III, whereas the PKP group included 3 cases of stage I, 17 cases of stage II, and 5 cases of stage III (Table 1).

2.2 | Surgical procedures

All surgeries conducted under local anesthesia using a unilateral or bilateral pedicle approach for PKP and HPS-KP. Balloon dilatation was performed strictly under C-arm fluoroscopy to restore the height of the vertebral body and expand the IVC. To ensure that the doughy stage (resembling toothpaste in consistency) polymethylmethacrylate cement (PMMA, Ningbo City, Zhejiang Province, China) was filled in the IVC. Intraoperative monitoring from the C-arm fluoroscopy was conducted to determine whether bone cement leakage occurred during the injection of bone cement into the vertebral body.

FIGURE 1 Follow-up scheme. PKP group (treated with percutaneous kyphoplasty; $n = 25$) and HPS-KP group (treated with a novel hollow pedicle screw combined with kyphoplasty; $n = 25$), respectively.
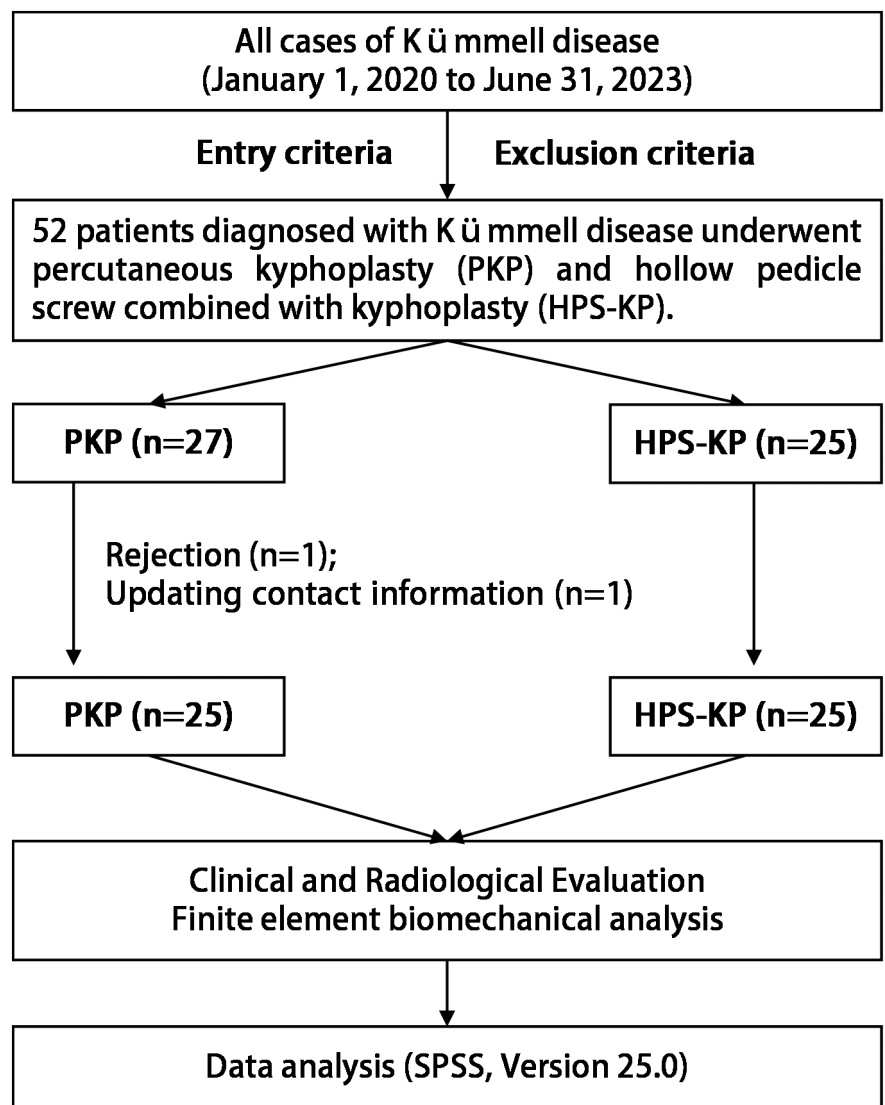
All cases of K ü mmell disease
(January 1, 2020 to June 31, 2023)

Entry criteria | Exclusion criteria

52 patients diagnosed with K ü mmell disease underwent percutaneous kyphoplasty (PKP) and hollow pedicle screw combined with kyphoplasty (HPS-KP).

PKP (n=27) | HPS-KP (n=25)

Rejection (n=1);
Updating contact information (n=1)

PKP (n=25) | HPS-KP (n=25)

Clinical and Radiological Evaluation
Finite element biomechanical analysis

Data analysis (SPSS, Version 25.0)

TABLE 1 Baseline data of the two groups.

| Variables		PKP ($n = 25$)	HPS-KP ($n = 25$)	U/X^2	p values
Age		70.00 (67.00, 75.50)	73.00 (68.50, 79.00)	$U = 370$	0.262
Intraoperative blood loss (mL)		9 (7, 10)	10 (9, 15)	$U = 492.50$	<0.001
Bone cement volume		5 (4, 6)	4 (3, 6)	$U = 211.50$	0.043
Bone mineral density (T-score, g/cm^3)		−3.00 (−3.80, −2.50)	−3.20 (−3.85, −2.50)	$U = 290.50$	0.664
Follow-up time		24 (14, 24)	14 (12.5, 21.5)	$U = 207.50$	0.035
Gender	Female	20 (80%)	17 (68.0%)	$X^2 = 0.936$	0.333
	Male	5 (20%)	8 (32.0%)		
Unilateral/bilateral surgery	Unilateral	6 (24%)	18 (72.0%)	$X^2 = 11.538$	<0.001
	Bilateral	19 (76%)	7 (28.0%)		
Staging	Stage I	3 (12%)	3 (12.0%)	$X^2 = 3.533$	0.148
	Stage II	17 (68%)	11 (44.0%)		
	Stage III	5 (20%)	11 (44.0%)		
Complications	Bone cement leakage	8 (32%)	6 (24.0%)	$X^2 = 0.397$	0.529
	Adjacent vertebral fractures	4 (16%)	1 (4.0%)	$X^2 = 0.889$	0.346
	Bone cement displacement	2 (8%)	0	$X^2 = 0.521$	0.470
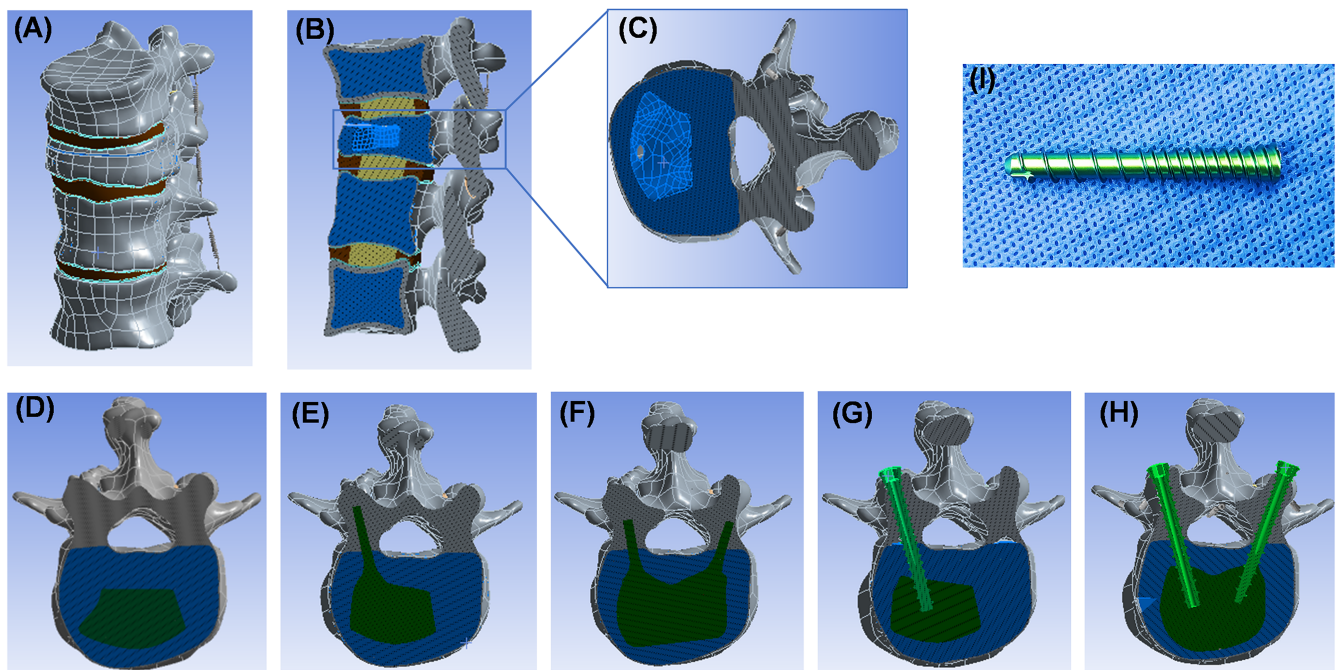
FIGURE 2   (A) and (B) Axial and sagittal views of the T11-L2 3D model and T12 fracture model, respectively. (C) A compression fracture with intravertebral vacuum cleft model (M1). (D) A simple unilateral percutaneous kyphoplasty (PKP) model (M2). (E) A unilateral PKP combined with pediculoplasty model (M3). (F) A bilateral PKP combined with pediculoplasty model (M4). (G) A unilateral hollow pedicle screw combined with the kyphoplasty model (M5). (H) A bilateral hollow pedicle screw combined with the kyphoplasty model (M6). (I) Physical drawing of the novel hollow pedicle screw.

Subsequently, the percutaneous hollow pedicle screws (Figure 2I. TC4 material, Geasure Medical Apparatus and Instruments Co., Ltd., Changzhou, Jiangsu Province, China) with diameters ranging from 5.0 to 6.0 mm and lengths ranging from 30 to 60 mm were promptly implanted into the affected vertebrae before solidification of PMMA. These screws were fully interlocked with the cement block to effectively prevent any potential loosening or displacement of the cement. Finally, the efficacy of PMMA reinforcement and screw fixation was evaluated again via C-arm fluoroscopy. The specific surgical procedure is shown in Figure 3B.

2.3 | Outcome assessment

The basic information of patients, intraoperative blood loss, bone cement volume, and bone mineral density (BMD, T-score) were obtained from the medical records. Visual analogue scale (VAS, 0 score: no pain; 10 score: the heaviest pain) and Oswestry dysfunction index (ODI, 100%: best functional state; 0%: worst functional state; the sexual evaluation was removed) at preoperative, 3 days, 3 and 6 months, and 1 year after operation were used to evaluate the extent of pain relief. The anterior vertebral height (AVH), wedge-shaped vertebral Cobb angle (WCA), and biarticulate vertebral Cobb angle (BCA) were measured at preoperative, initial postoperative and final follow-up (Figure 3A).

Additionally, the incidence of postoperative complications conducted as well.

2.4 | Development of an intact thoracolumbar finite element model

The spine of a 77-year-old KD female patient undergone bilateral PKP surgery was scanned with a Siemens 16-slice spiral CT (Type: SOMA-TOM Emotion. Device serial number: 32263, and manufactured in 2007 in Germany) at 130 kV, automatic tube current modulation (ATCM), and 1 mm thickness after obtaining informed consent. The CT data were extracted in a 512×512 pixels DICOM format, and first imported into Mimics 21.0 (Materialize Mimics, Belgium) for pre-processing, and then a preliminary T11-L2 3D model was established. Second, the model was further smoothed, polished, restored, and reconstructed using Geomagic wrap 2017 (Raindrop Inc., Mabhilhi, USA) and SolidWorks 2017 software (Dassault Inc., France) to obtain a more accurate model. Finally, the model was meshing, material property assignment, and finite element analysis in Ansys 17.0 (ANSYS Inc., Pittsburgh, PA, USA). The finite element model of T11-L2 was constructed by the general steps mentioned above (Figure 2A,B). Including six models: model 1 is the compression fracture vertebral body with IVC (M1, Figure 2C), model 2 is simply unilateral PKP (M2, Figure 2D), model 3 is unilateral PKP combined with pediculoplasty
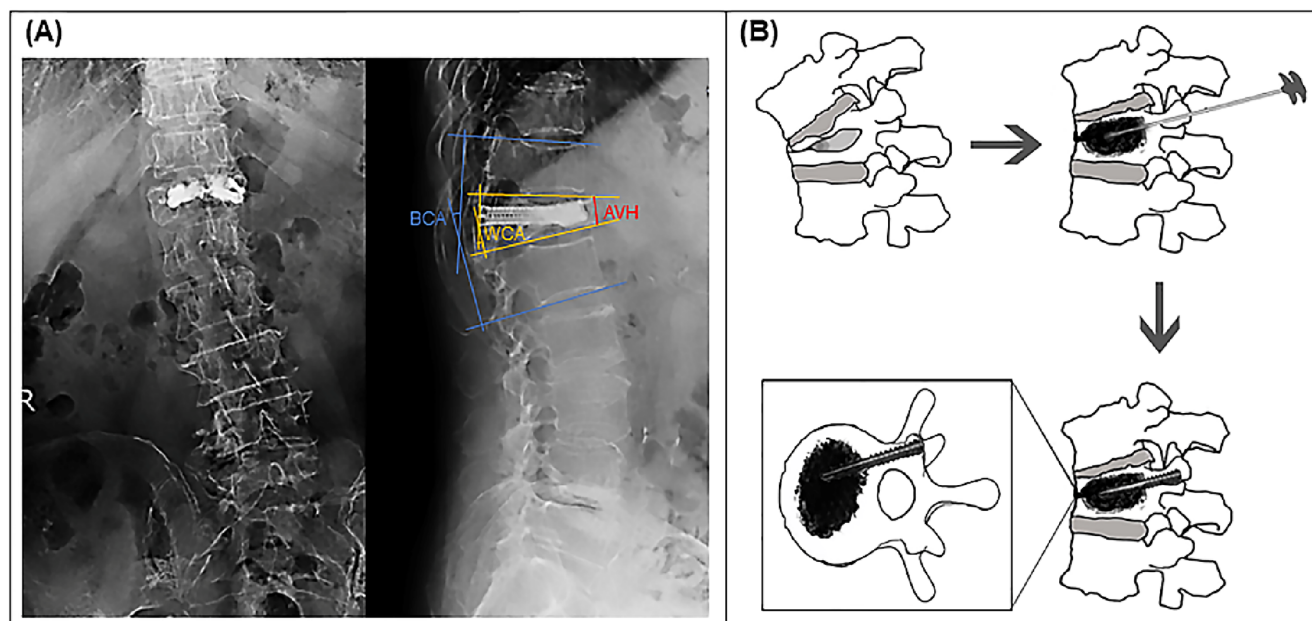
FIGURE 3 (A) The postoperative anteroposterior (Left) and lateral (Right) radiograph of KD treated with two novel hollow pedicle screws combined with kyphoplasty. AVH: The anterior vertebral height. WCA: The wedge-shaped vertebral Cobb angle. BCA: The biarticulate vertebral Cobb angle. (B) A specific surgical procedure.

(M3, Figure 2E), model 4 is bilateral PKP combined with pediculoplasty (M4, Figure 2F), model 5 is unilateral HPS-KP (M5, Figure 2G), and model 6 is bilateral HPS-KP (M6, Figure 2H).

2.5 | Vertebra models with KD

Given that KD primarily affects the thoracolumbar junction and the IVC sign is crucial, we developed a KD model with IVC by removing portions of bone from the T12 vertebral body using SolidWorks 2017 software (Dassault Inc., France). To replicate the IVC and vertebral body fracture, a 1 mm-thick incision connected to an irregular cavity measuring 4 cm^3 in the anterior and middle columns of the T12 vertebral body (Figure 2B,C).

2.6 | Material properties and contact types

The elastic modulus of all bone structures was reduced to 67% in cortical bone and to 34% in cancellous bone and cartilaginous endplates, compared with normal bone.[20] Due to the limitation of their structural characteristics, the resolution of flexible structures in the bone window level of CT is low, and it is difficult to extract the flexible structures, which rely on high-quality MRI data for extraction. This experiment is based on the simulation of thoracolumbar CT data, which cannot be extracted directly and needs to be reconstructed in SolidWorks 2017 software (Dassault Inc., France). The generation of the intervertebral disc was based on the datum of the grid structure of the vertebral surface, and the plane profile of the intervertebral disc was drawn with the help of the measurement command. The

"Stretch-convex" command and the "isometric surface" command were used to construct the intervertebral disc structure. However, the nucleus pulposus structure was outside the interior of the intervertebral disc, and the volume of the nucleus pulposus accounted for 50% of the volume of the intervertebral disc measured by the measuring tool. The size of the preliminarily constructed nucleus pulposus and annulus fibrosus was adjusted to close to the real nucleus pulposus volume, and then the annulus fibrosus and nucleus pulposus were generated by cutting with an isometric surface. In addition, the upper and lower cartilage endplates were separated from the three-dimensional disc structure. The thickness of the cartilage endplate is 1 mm. By using the "Equidistant surface" command, the thickness of the equidistant surface was adjusted to 1 mm to approximate the thickness of the cartilage endplate in the real anatomical structure. With the help of the "Move copy entity/compose" command, the cortical bone shell and cancellous bone core were separated to replicate the cancellous bone entities and cement masses of T11, T12, L1, and L2. The essence of the "Compose" command is to delete the overlapping part of cortical bone with internal cancellous bone and cement, and obtain a simple cortical bone shell and internal cancellous bone and cement masses, thereby improving the simulation of the model.

According to the previous literature[21–23] on KD, the material properties specific to the models were assigned in Ansys 17.0 (Table 2). Spring elements were used to replace the physiological ligament structure in Ansys17.0 software (Figure 2A). To make the model structure accurate, the tetrahedral mesh was used to divide the model in Ansys, and the grid element type of these models were ten-node tetrahedral element (C_4H_{10}). The contact type between the models was defined in connection. Reasonable contact between structures is a necessary prerequisite for stress transfer, and the

TABLE 2   Material properties of finite element analysis models.

Material	Young modulus (MPa)	Poisson ratio	Stiffness coefficient (N/mm)
Cortical bone	8040 (67% normal)	0.3	-
Cancellous bone	34 (34% normal)	0.25	-
Cartilage	10 (67% normal)	0.4	-
Cartilaginous endplate	670 (67% normal)	0.4	-
Annulus	4.2	0.45	-
Nucleus pulposus	1	0.49	-
Bone cement (PMMA)[a]	3000	0.4	-
Pedicle screws and rods	110 000	0.3	-
Ligaments			
Anterior longitudinal ligament	-	-	33
Posterior longitudinal ligament	-	-	20.4
Supraspinous ligament	-	-	23.7
Ligamentum flavum	-	-	27.2
Intertransverse ligament	-	-	15
Interspinous ligament	-	-	11.5

[a]Polymethylmethacrylate.

contact relationship mainly includes fixed contact and limited contact. "Surface-surface contact" and "Point-surface contact" are the main forms of model contact, and the contact relationship can be set through the connection command. The vertebral body-endplate, cortical bone-cancellous bone, and endplate-intervertebral disc were set as bonded mode. The articular cartilage had a certain range of motion but would not deviate from the motion track, and its contact was a limited contact within a certain range of frictionless displacement sliding. Therefore, the contact mode was set to the no-separation mode.

2.7 | Boundary conditions and loads

All models were fixed at the bottom of the L2 vertebral body (six-way displacement was 0). The loads were allocated from the upper endplate of the T11 vertebral body according to the theory of three columns of the spine, in which 85% of the weight load is carried by the anterior and middle column, and about 15% is carried by the elements behind the vertebrae.[22] An axial compressive load of 500 N was applied to the upper surface of the T11 vertebral body to simulate the weight of the human upper body segment, and a pure moment of 7.5 Nm combined with a pre-compressive load of 500 N was applied to perform axial load, flexion, extension, left/right bending, and left/right axial rotation.[22,24] After loading boundary conditions, finite element analysis was carried out on the models.

2.8 | Statistical analysis

SPSS 25.0 software (Chicago, USA) was used for statistical analysis. The Shapiro–Wilk test revealed that the age, intraoperative blood loss, bone cement volume, bone mineral density, and follow-up

time in both groups exhibited a non-normal distribution, which was described by median and percentile. However, the VAS, ODI, AVH, BCA, and WCA indicators followed a normal distribution, and the data were described by mean values and standard deviations. The Mann–Whitney U test and X^2 test were used to compare the differences in baseline data between the two groups. Additionally, a two-factor repeated measurement analysis of variance was conducted to analyze the efficacy indicators of the two groups, including VAS, ODI, AVH, BCA, and WCA. If Mauchly's test of sphericity was met, the variance value of sphericity was adopted; otherwise, the corrected result in one-way analysis of variance "Greenhouse–Geisser" was used as the standard. Bonferroni adjusted p values were used for pairwise comparisons. $p < 0.05$ was considered statistically significant.

3 | RESULTS

3.1 | General data

The bone cement volume of the HPS-KP and PKP groups was 4 (3, 6) mL and 5 (4, 6) mL, respectively ($p = 0.043$). The intraoperative blood loss of the HPS-KP group was 10 (9, 15) mL and that of the PKP group was 9 (7, 10) mL ($p < 0.001$). The BMD value was −3.20 (−3.85, −2.50) g/cm^3 for the HPS-KP group and −3.00 (−3.80, −2.50) g/cm^3 for the PKP group ($p = 0.664$). The follow-up time was 24 (14, 24) months and 14 (12.5, 21.5) months in PKP and HPS-KP groups, respectively ($p = 0.035$, Table 1). Though the HPS-KP group had a lower cement leakage rate (24.0%) than the PKP group (32%) ($p = 0.529$) and had a lower incidence of adjacent vertebral refracture (4.0%) than the PKP group (16%) ($p = 0.346$), they were not statistically different. No bone cement leakage from the posterior edge of

TABLE 3 Comparison of VAS and ODI between the two groups.

Time point	VAS (score)		ODI (%)	
	PKP (n = 25)	HPS-KP (n = 25)	PKP (n = 25)	HPS-KP (n = 25)
Preoperative	7.00 ± 0.65	6.88 ± 0.67	71.73 ± 8.40	73.33 ± 9.43
3 days postoperative	2.24 ± 0.72[a]	2.28 ± 0.54[a]	33.16 ± 7.59 [a]	33.24 ± 7.87 [a]
3 months postoperative	1.08 ± 076[a,b]	1.24 ± 0.72[a,b]	22.49 ± 6.89[a,b]	23.82 ± 7.22[a,b]
6 months postoperative	1.32 ± 0.90[a,b]	1.24 ± 0.83[a,b]	23.02 ± 8.84[a,b]	23.02 ± 7.88[a,b]
1 year postoperative	1.04 ± 0.79[a,b]	1.08 ± 0.64[a,b]	19.91 ± 5.97[a,b]	22.49 ± 6.65[a,b]
RM-ANOVA				
Time (F, P, η^2)	826.523, 0.000, 0.945		839.128, 0.000, 0.946	
Intergroup (F, P, η^2)	0.004, 0.953, 0.000		0.419, 0.520, 0.009	
Interaction (F, P, η^2)	0.405, 0.773, 0.008		0.525, 0.666, 0.011	

Note: The "a" in the upper right corner indicates statistically significant difference compared with preoperative ($p < 0.001$), and "b" indicates statistically significant difference compared with 3 days postoperative ($p < 0.001$).
Abbreviations: ODI, Oswestry dysfunction index; VAS, visual analogue scale.

the vertebral body into the spinal canal, and no clinical symptoms caused by bone cement leakage were observed in both groups. In the PKP group, two cases had signs of cement displacement at the last imaging compared with the initial postoperative imaging, but there were no corresponding clinical symptoms. However, no cement displacement was observed in the HPS-KP group (Table 1).

3.2 | Clinical efficacy scores and radiographic outcomes

Two-way repeated measures analysis of variance results demonstrated that there was no interaction between group and time in terms of VAS score and ODI score ($F_{time*group} = 0.405$, $p = 0.773$, partial $\eta^2 = 0.008$; $F_{time*group} = 0.525$, $p = 0.666$, partial $\eta^2 = 0.011$), thus the main effect analysis was carried out. Statistically significant differences in VAS score and ODI score were observed between the two groups at different time points ($F_{time} = 826.523$, $p < 0.001$, partial $\eta^2 = 0.945$; $F_{time} = 839.128$, $p < 0.001$, partial $\eta^2 = 0.946$), whereas there was no significant difference in VAS score and ODI between the two surgical methods in KD patients ($F_{group} = 0.004$, $p = 0.953$, partial $\eta^2 = 0$; $F_{group} = 0.419$, $p = 0.52$, partial $\eta^2 = 0.009$). The VAS and ODI scores of both groups at 3 days, 3 months, 6 months, and 1 year after the operation were significantly improved compared with those before the operation ($p < 0.001$). The VAS and ODI scores at 3 months, 6 months, and 1 year after the operation were also significantly improved compared with those at 3 days after the operation ($p < 0.001$). In the PKP group, the VAS score decreased from (7.00 ± 0.65) score before the operation to (2.24 ± 0.72) score at 3 days after the operation, and the ODI score decreased from (71.73 ± 8.40)% before the operation to (33.16 ± 7.59)% at 3 days after the operation ($p < 0.001$). In the HPS-KP group, the VAS score decreased from (6.88 ± 0.67) score before the surgery to (2.28 ± 0.54) score at 3 days after the surgery, and the ODI score decreased from (73.33 ± 9.43)% before the surgery to (33.24

± 7.87)% at 3 days after the surgery ($p < 0.001$), as shown in Table 3 and Figure 4A,B.

Two-way repeated measures analysis of variance results demonstrated that there was no interaction between group and time in AVH and WCA between the two groups ($F_{time*group} = 1.467$, $p = 0.236$, partial $\eta^2 = 0.03$; $F_{time*group} = 0.991$, $p = 0.361$, partial $\eta^2 = 0.02$), thus the main effect analysis was carried out. There were significant differences in AVH and WCA between the two groups at different time points ($F_{time} = 64.29$, $p < 0.001$, partial $\eta^2 = 0.573$; $F_{time} = 50.524$, $p < 0.001$, partial $\eta^2 = 0.513$), but there was no significant difference in AVH and WCA between the two surgical methods in KD patients ($F_{group} = 0.89$, $p = 0.35$, partial $\eta^2 = 0.018$; $F_{group} = 0.021$, $p = 0.887$, partial $\eta^2 < 0.001$). The AVH and WCA of the two groups were significantly improved after the initial operation and at the last follow-up ($p < 0.05$), but the AVH and WCA at the last follow-up were worse than those at the initial operation ($p < 0.05$). In the PKP group, AVH and WCA improved from (17.58 ± 3.79) mm and (14.76 ± 5.40)° to (22.22 ± 3.51) mm and (9.72 ± 4.58)° respectively (All $p < 0.05$). In the HPS-KP group, the AVH and WCA changed from (16.79 ± 5.66) mm and (15.08 ± 7.30)° to (20.32 ± 5.24) mm and (9.80 ± 5.02)° respectively (All $p < 0.05$), as shown in Table 4 and Figure 4C,D.

Two-way repeated measures analysis of variance showed that there were statistically significant differences between the two groups of patients with BCA at different time points ($F_{time} = 31.947$, $p < 0.001$, partial $\eta^2 = 0.4$). However, for KD patients, there was no statistically significant difference between the two surgical methods ($F_{group} = 1.502$, $p = 0.226$, partial $\eta^2 = 0.03$). Additionally, an interaction between group and time was observed ($F_{time*group} = 3.758$, $p = 0.027$, partial $\eta^2 = 0.073$), thus the simple effect analysis was carried out. The simple effect results showed that BCA in the PKP group was statistically different at different time points ($F_{time} = 13.276$, $p < 0.001$, partial $\eta^2 = 0.361$), and the same was true in the HPS-KP group ($F_{time} = 37.308$, $p < 0.001$, partial $\eta^2 = 0.614$). There was no significant difference in BCA between the PKP and HPS – KP groups
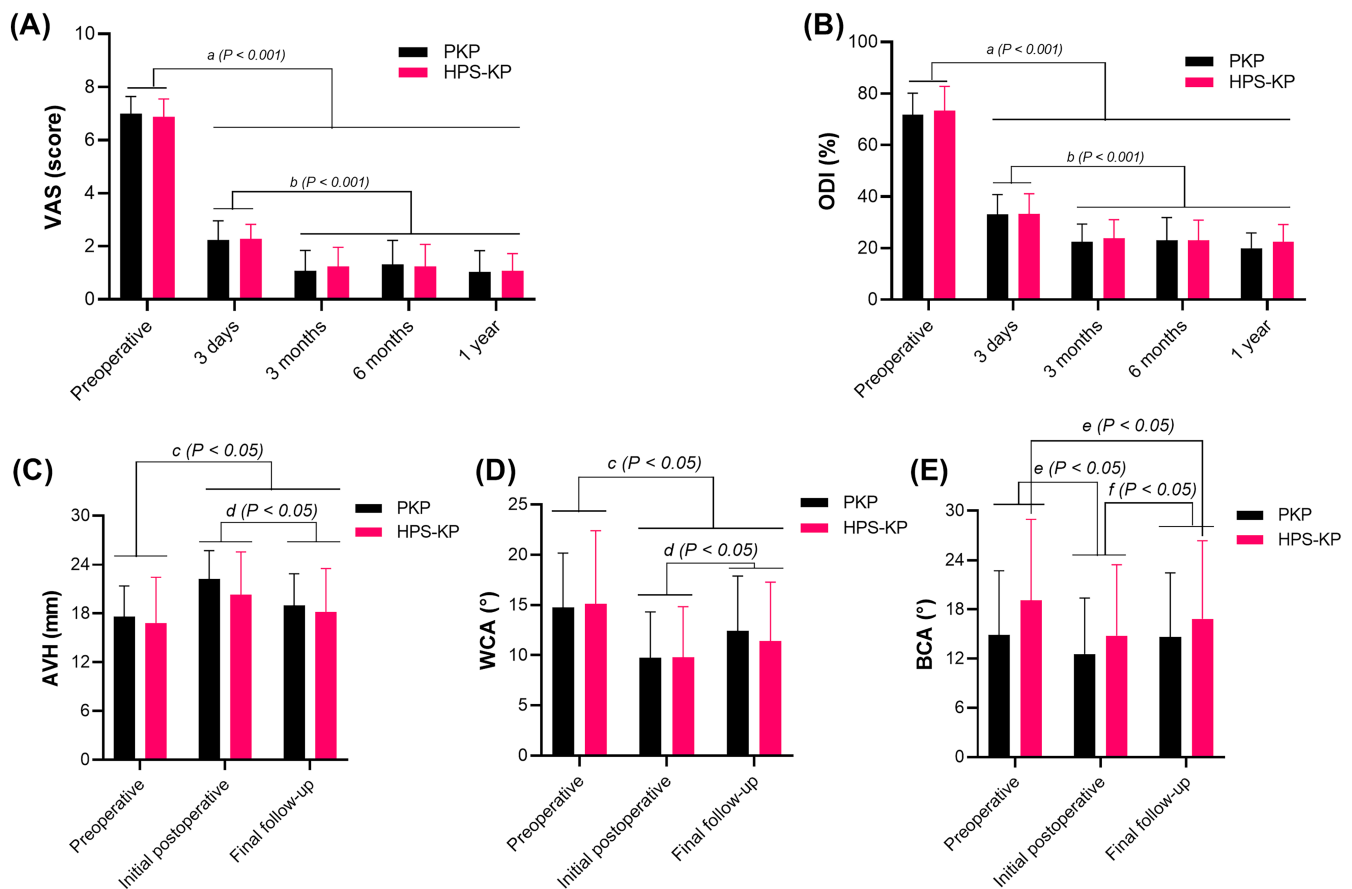
FIGURE 4 The comparison of VAS scores (A), ODI scores (B), AVH (C), WCA (D), and BCA (E) at different times in both groups. "a" indicates the statistical difference compared with the preoperative ($p < 0.001$), and "b" indicates the statistical difference compared with the postoperative 3 days ($p < 0.001$), and "c" and "e" indicate the statistical difference compared with the preoperative ($p < 0.05$), and "d" and "f" indicate the statistical difference compared with the initial postoperative ($p < 0.05$).

TABLE 4 Comparison of AVH and WCA between the two groups.

Time point	AVH (mm)		WCA (°)	
	PKP ($n = 25$)	HPS-KP ($n = 25$)	PKP ($n = 25$)	HPS-KP ($n = 25$)
Preoperative	17.58 ± 3.79	16.79 ± 5.66	14.76 ± 5.40	15.08 ± 7.30
Initial postoperative	22.22 ± 3.51[c]	20.32 ± 5.24[c]	9.72 ± 4.58[c]	9.80 ± 5.02[c]
Final follow-up	19.00 ± 3.88[c,d]	18.16 ± 5.36[c,d]	12.44 ± 5.43[c,d]	11.40 ± 5.87[c,d]
RM-ANOVA				
Time (F, P, η^2)	64.29, 0.000, 0.573		50.524, 0.000, 0.513	
Intergroup (F, P, η^2)	0.890, 0.350, 0.018		0.021, 0.887, 0.000	
Interaction (F, P, η^2)	1.467, 0.236, 0.030		0.991, 0.361, 0.020	

Note: The "c" in the upper right corner indicates statistically significant difference compared with preoperative ($p < 0.05$), and "d" indicates statistically significant difference compared with initial postoperative ($p < 0.05$).

Abbreviations: AVH, anterior vertebral height, WCA, wedge-shaped vertebral Cobb angle.

before the operation, after the initial operation, and at the last follow-up ($F_{group} = 2.772$, $p = 0.102$, partial $\eta^2 = 0.055$; $F_{group} = 1.038$, $p = 0.313$, partial $\eta^2 = 0.021$; $F_{group} = 0.798$, $p = 0.376$, partial $\eta^2 = 0.016$). The BCA of both groups was significantly improved after the initial surgery ($p < 0.05$) but deteriorated at the final follow-up ($p < 0.05$). There was no significant difference between the preoperative and final follow-up in the PKP group ($p > 0.05$), whereas there was a significant difference in the HPS-KP group ($p < 0.05$). In the PKP group, the BCA increased from (14.88 ± 7.81)° before the operation to (12.56 ± 6.80)° after the initial operation ($p < 0.05$), whereas in the HPS-KP group, the BCA increased from (19.08 ± 9.90)° to (14.80 ± 8.64)° ($p < 0.05$), as shown in Table 5 and Figure 4E.

TABLE 5 Comparison of BCA between the two groups.

Time point	BCA (°)		Simple effect Intergroup (F, P, η^2)
	PKP (n = 25)	HPS-KP (n = 25)	
Preoperative	14.88 ± 7.81	19.08 ± 9.90	2.772, 0.102, 0.055
Initial postoperative	12.56 ± 6.80 [e]	14.80 ± 8.64 [e]	1.038, 0.313, 0.021
Final follow-up	14.64 ± 7.81 [f]	16.84 ± 9.52 [e,f]	0.798, 0.376, 0.016
Simple effect			
Time (F, P, η^2)	13.276, 0.000, 0.361	37.308, 0.000, 0.614	
RM–ANOVA (main effect)			
Time (F, P, η^2)	31.947, 0.000, 0.400		
Intergroup (F, P, η^2)	1.502, 0.226, 0.030		
Interaction (F, P, η^2)	3.758, 0.027, 0.073		

Note: The "e" in the upper right corner indicates statistically significant difference compared with preoperative ($p < 0.05$), and "f" indicates statistically significant difference compared with initial postoperative ($p < 0.05$).

Abbreviation: BCA, biarticulate vertebral Cobb angle.

3.3 | Model validation

Once the model is successfully established, the finite element software is used for calculation. Before the biomechanical experiment, biomechanical verification of the three-dimensional finite element model is a necessary prerequisite for validating the accuracy and reliability of the model. The validity verification methods for spine finite element models mainly comprise direct verification and indirect verification. Direct verification requires verification with an ex vivo model, which is reliable yet difficult. Indirect verification involves comparing the angular displacement of the finite element model with that of previous biomechanical experiments. In this experiment, the maximum angular displacement of the model in each direction, namely the range of motion (ROM), was recorded. Then, by referring to the results of the standard spine finite element experiment and biomechanical experiment, the flexion change of the constructed model was compared to determine the effectiveness of the constructed model and whether it can be applied to further model processing and finite element analysis. The present model results were in good agreement with the results obtained from the literature (Lu et al.[23] and Panjabi et al.[25]), and the model verification results are shown in Figure 5F. This model adopts an accurate modeling path with fine division of grids and elements, possessing a high degree of simulation, strong accuracy, and qualified validity verification.

3.4 | The maximum von Mises stress and stress distributions on T12

Figure 5C shows the maximum von Mises stress on T12 in the six models. The von Mises stress of T12 demonstrated an increasing tendency during both forward and left bending. Among all models, the maximum von Mises stress of T12 in M1 under 7 different loading directions was the largest, which was 83.757, 120.94, 46.586, 124.1,

115.57, 81.762, and 85.951 MPa in axial compression, flexion, extension, left/right bending, and left/right rotation, respectively. After KD underwent surgery, the maximum von Mises stress of T12 of M2 was significantly greater than that of other models under 7 different loading directions. Particularly in the left bending, the maximum von Mises stress of T12 gradually decreased from M2 to M6, which was 89.023, 73.002, 57.050, 45.954, and 32.604 MPa, respectively. In addition, the stress of T12 in M6 was the minimum under 7 different loading directions, which was 21.521, 36.301, 19.997, 32.604, 21.738, 21.078, and 31.897 MPa in axial compression, flexion, extension, left/right bending, and left/right axial rotation, respectively (Table 6). Figure 6 illustrates the stress distributions of the 6 models at T12 (different color areas, with colors closer to red indicating higher von Mises stress values and closer to blue indicating lower von Mises stress values). Under the six loading conditions (the flexion, extension, left/right bending, and left/right rotation), the stress in M1 was mainly concentrated in the anterior column of T12, and the stress distribution area (the area of the red area) was significantly larger than that of the other models. There was no obvious difference between M2 and M3, but the stress distribution of unilateral M3 and M5 was mainly concentrated on the unreinforced side of the bone cement (the left side of the vertebral body, near the bottom side of the model in Figure 6), whereas the stress distribution of bilateral M4 and M6 was symmetrical.

3.5 | The maximum von Mises stress on T11 and L1

As depicted in Figure 5A,B, in the flexion, left and right bending of the six models, the von Mises stress of the adjacent T11 and L1 presented an increasing trend. The change trend of M1 was nearly identical to that of the M2, and both were significantly larger than those of the other models. No significant differences in von Mises stress between
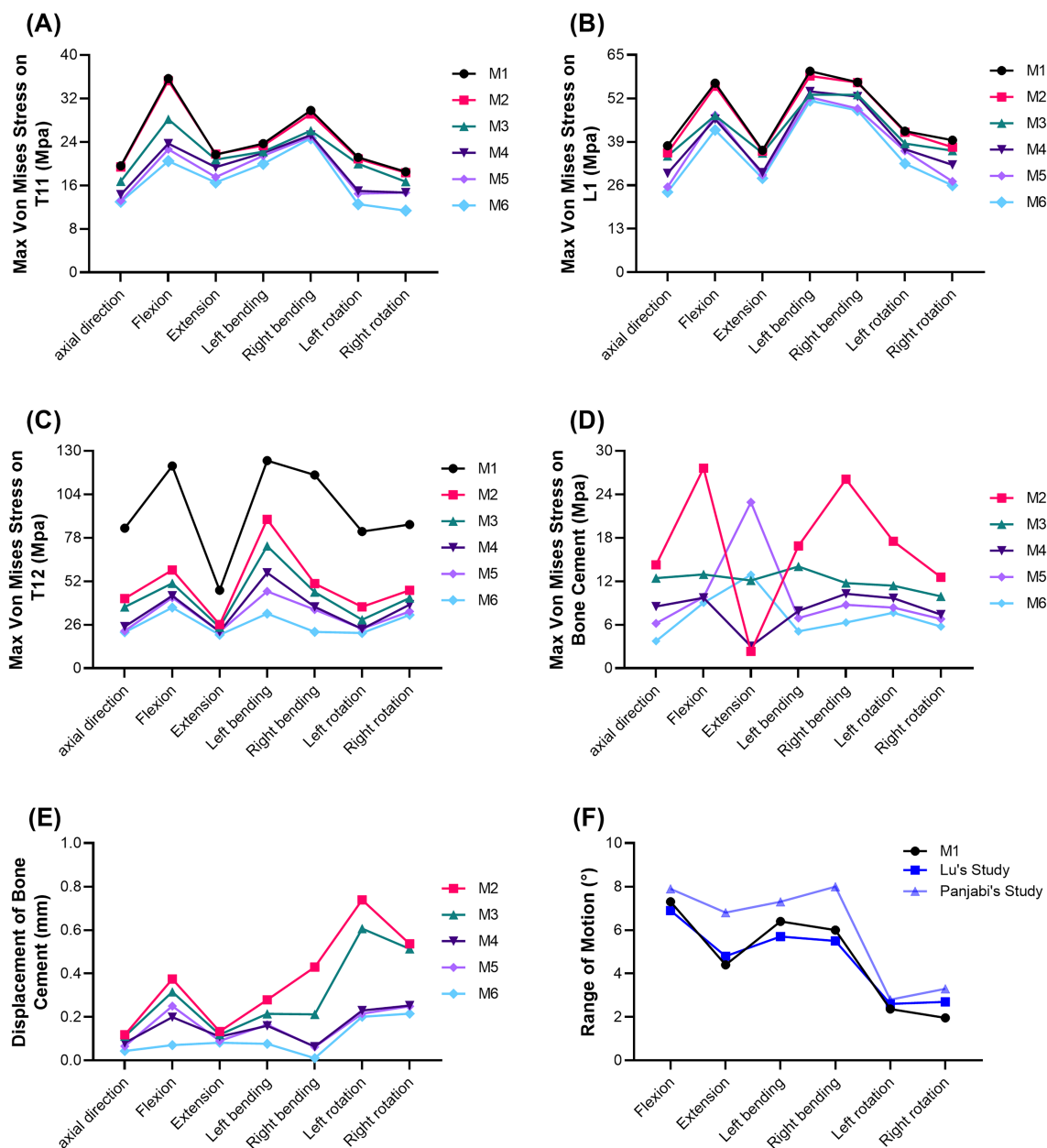
FIGURE 5 (A) The maximum von Mises Stress on T11 in M1 to M6 under seven conditions (axial direction, flexion, extension, left and right bending, left and right rotation). (B) The maximum von Mises Stress on L1 in M1 to M6 under seven conditions. (C) The maximum von Mises Stress on T12 in M1 to M6 under seven conditions. (D) The maximum von Mises Stress on bone cement in M2 to M6 under seven conditions. (E) The displacement distance of bone cement in M2 to M6 under seven conditions. (F) The validation of the models under six conditions (flexion, extension, left and right bending, left and right rotation).

T11 and L1 were found in the M3, M4, M5, and M6 models. Additionally, the von Mises stresses of the adjacent T11 and L1 in M6 were the smallest. The von Mises stresses of T11 in axial compression, flexion, extension, left/right bending, and left/right rotation were 12.979, 20.458, 16.529, 19.964, 24.680, 12.554, and 11.363 MPa respectively, whereas those of L1 were 23.951, 42.508, 28.083, 51.251, 48.391, 32.522, and 25.97 MPa, respectively (Table 6). It is worth noting that from M1 to M6, the von Mises stresses of T11 and L1 gradually decreased during forward flexion, and the overall stress values of L1 were larger than those of T11 (Table 6).

3.6 | The maximum von Mises stress and stress distribution on bone cement

As depicted in Figure 5D, the stress of M2 bone cement was significantly higher than that of the other models under six loads except for extension. Particularly in flexion and right bending, the stresses were 27.592 and 26.079 MPa respectively. The von Mises stresses of M3, M4, and M5 also decreased successively under the six loads except for extension. The von Mises stress of M6 remained the smallest, which was 3.737, 9.019, 5.085, 6.319, 7.648, and 5.762 MPa in axial

TABLE 6 Comparison of the maximum von Mises stress on T11, T12, L1, and bone cement in all models (MPa).

Loads direction	Projects	M1	M2	M3	M4	M5	M6
Axial compression	T11	19.594	19.374	16.762	14.308	13.196	12.979
	T12	83.757	41.688	36.647	24.902	22.239	21.521
	L1	37.837	35.717	34.735	29.573	25.514	23.951
	Bone cement	-	14.273	12.441	8.5178	6.183	3.7367
Flexion	T11	35.659	35.235	28.153	23.704	22.641	20.458
	T12	120.940	58.780	50.768	43.342	42.258	36.301
	L1	56.535	55.590	46.850	45.743	46.995	42.508
	Bone cement	-	27.592	12.937	9.726	9.808	9.019
Extension	T11	21.667	21.750	20.729	19.371	17.525	16.529
	T12	46.586	26.125	24.445	21.858	21.875	19.997
	L1	36.442	36.199	35.653	29.806	29.104	28.083
	Bone cement	-	2.317	12.094	3.023	22.888	12.884
Left bending	T11	23.682	23.329	22.194	21.970	21.462	19.964
	T12	124.100	89.023	73.002	57.050	45.954	32.604
	L1	60.102	58.712	53.092	54.071	52.319	51.251
	Bone cement	-	16.871	14.043	7.920	6.931	5.0847
Right bending	T11	29.793	29.131	26.059	25.246	24.954	24.680
	T12	115.570	50.584	45.509	36.754	35.077	21.738
	L1	56.815	56.721	53.072	52.552	48.981	48.391
	Bone cement	-	26.079	11.743	10.278	8.738	6.319
Left rotation	T11	21.159	20.866	19.981	14.975	14.483	12.554
	T12	81.762	36.715	29.023	23.475	23.622	21.078
	L1	42.212	41.855	38.487	36.788	36.293	32.522
	Bone cement	-	17.506	11.392	9.657	8.369	7.648
Right rotation	T11	18.511	18.341	16.682	14.688	14.673	11.363
	T12	85.915	46.671	42.009	38.071	33.988	31.897
	L1	39.473	37.396	36.342	32.090	27.159	25.970
	Bone cement	-	12.563	9.919	7.409	6.786	5.763

Note: T11 represents the eleventh thoracic vertebra, T11 the twelfth thoracic vertebra, and L1 the first lumbar vertebra. M 1 is the compression fracture vertebral body with IVC model, M2 is simply unilateral PKP model, M3 is unilateral PKP combined with pediculoplasty model, M4 is bilateral PKP combined with pediculoplasty model, M5 is unilateral HPS-KP model, and M6 is bilateral HPS-KP model.

compression, flexion, left/right bending, and left/right rotation, respectively (Table 6). As shown in Figure 7, under the six loading conditions, it can be observed that the stress distribution of M3 and M4 was mainly concentrated at the junction between the screw and the cement block (where the screw is at the boundary between the cementless and cemented areas), whereas the stress distribution of M5 and M6 was mainly concentrated on the screw. The stress distribution of bilateral M4 and M6 was more symmetrical than that of unilateral M3 and M5.

3.7 | The displacement distance of the bone cement

As depicted in Figure 5E, all models exhibited an increasing trend in the cement displacement distance during forward flexion. Additionally, the

trends of M2 and M3 were nearly identical, showing an increase during flexion, left and right bending, and left rotation. Moreover, M2 and M3 were significantly larger than other models during right bending and left and right rotations. The displacements of M2 during right bending and left and right rotations were 0.430, 0.739, and 0.536 mm, respectively. The displacements of M3 during right bending and right and left rotations were 0.212, 0.607, and 0.513 mm, respectively (Table 7). The increasing trends of displacements of M4, M5, and M6 during flexion and left and right rotations were more prominent than those in other directions. There was no significant difference between M4 and M5 under the loading conditions in six aspects except for forward flexion. However, under seven loading conditions in different directions, the displacement distance of the M6 cement remained the smallest, which were 0.044, 0.071, 0.081, 0.077, 0.011, 0.201, and 0.215 mm during axial compression, flexion, extension, left/right bending, and left/right axial rotation, respectively (Table 7).
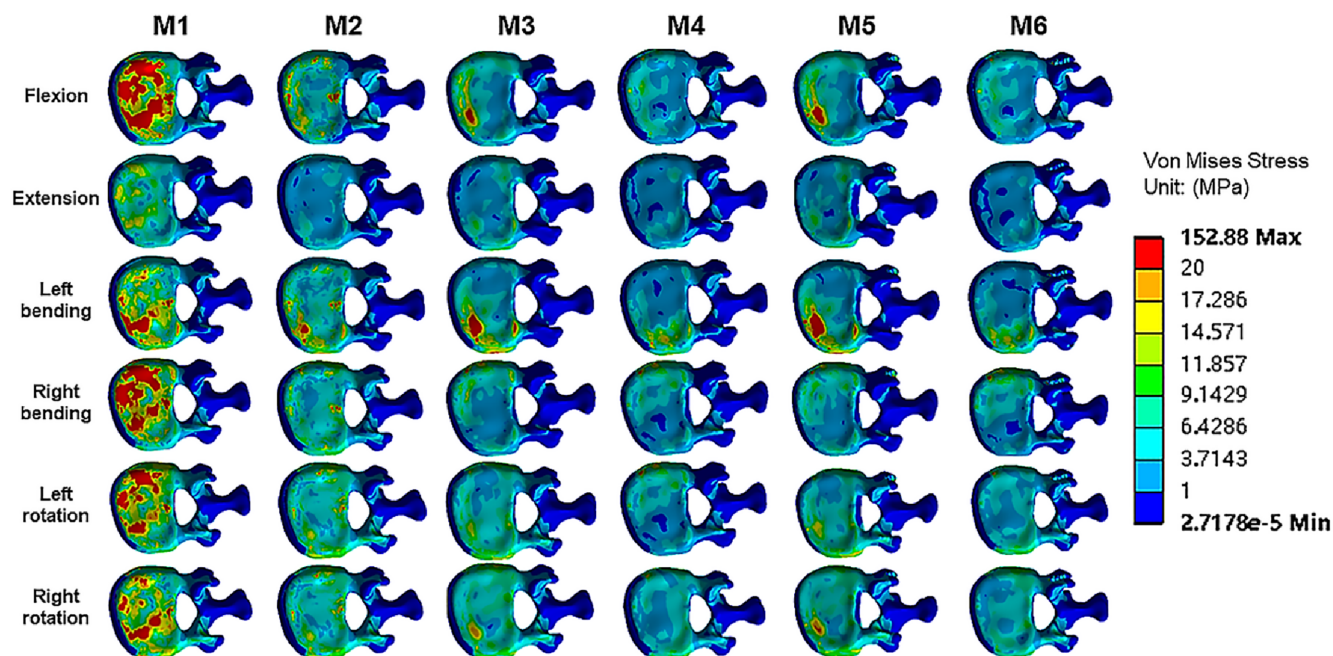
FIGURE 6 Stress distribution nephogram on T12 of M1 to M6 models under flexion and extension, left and right bending, and left and right rotation.
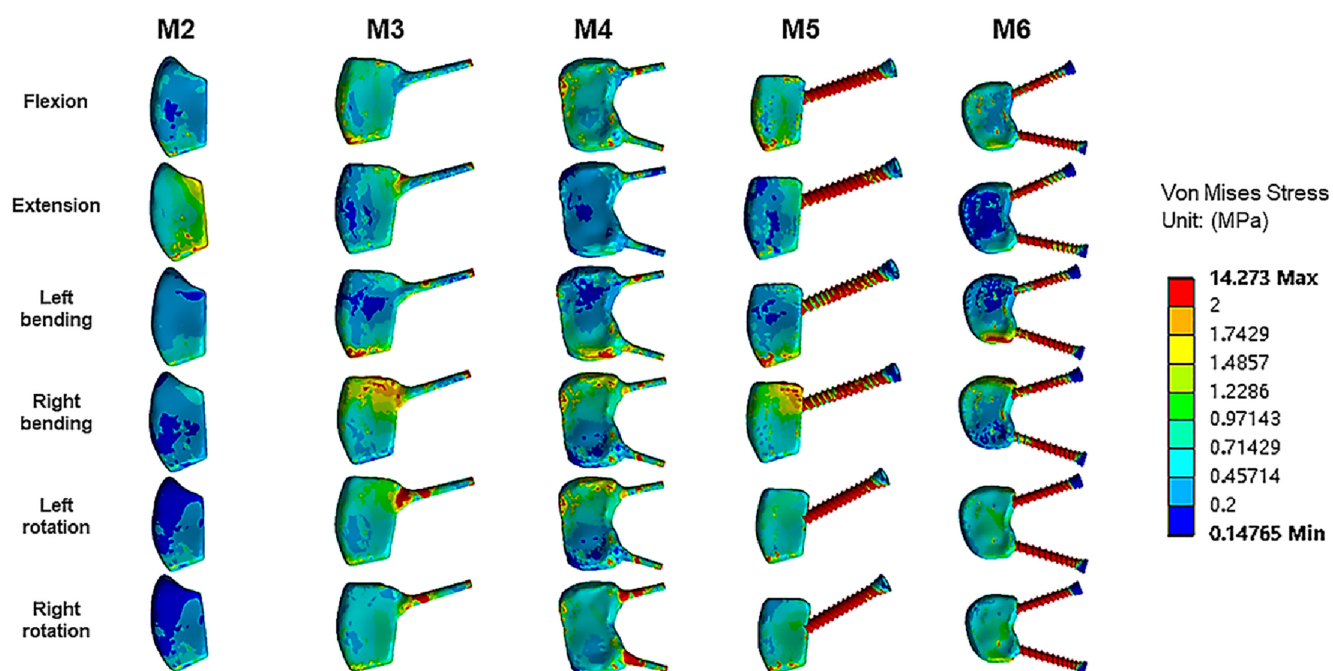

FIGURE 7 Stress distribution nephogram on bone cement of M2 to M6 models under flexion and extension, left and right bending, and left and right rotation.

4 | DISCUSSION

4.1 | The main clinical observations in KD patients

Although PKP/PVP are the main surgical interventions for KD and both can significantly relieve patients' pain, some studies have found that bone cement displacement occurs after PVP or PKP, resulting in serious problems that require treatment.[10,26,27] In this study, the HPS-KP used for KD achieved satisfactory clinical results. The VAS and ODI scores significantly improved after operation, and there was no difference between the two surgical methods. The HPS-KP and PKP have similar effects in relieving pain and improving quality of life, and

TABLE 7 Comparison of the displacement distance of the bone cement in M2 to M6 models (mm).

Loads direction	M2	M3	M4	M5	M6
Axial compression	0.118	0.111	0.081	0.066	0.044
Flexion	0.374	0.316	0.199	0.251	0.071
Extension	0.134	0.119	0.110	0.090	0.081
Left bending	0.279	0.214	0.160	0.165	0.077
Right bending	0.430	0.212	0.064	0.062	0.011
Left rotation	0.739	0.607	0.230	0.215	0.201
Right rotation	0.536	0.513	0.253	0.250	0.215

Note: M2 is simply unilateral PKP model, M3 is unilateral PKP combined with pediculoplasty model, M4 is bilateral PKP combined with pediculoplasty model, M5 is unilateral HPS-KP model, and M6 is bilateral HPS-KP model.

both they can restore vertebral height and improve local kyphosis. Unfortunately, the vertebral height and local kyphosis at last follow-up showed a trend of deterioration compared with those at initial postoperative. This study found that the recovery of vertebral height and kyphosis was about 14 to 24 months. In previous literatures, many studies[28,29] have reported recollapse of the augmented vertebrae with vertebral height loss and aggravation of kyphotic deformity after postoperative follow-up period. Some researchers[28,30] also suggested that preoperative IVC, solid lump cement distribution pattern, larger reduction rate, and larger reduction angle might be some important predisposing factors to recollapse.

4.2 | The causes of bone cement displacement and their different solutions

Gao et al.[10] have found that the thoracolumbar fracture, stage II KD, anterior cortex defect, uneven cement distribution, cement leakage, and high restoration of the local Cobb angle were risk factors for bone cement displacement after percutaneous vertebral augmentation in KD. Gao et al.[9] demonstrated that when the anterior vertebral cortex was defective, it would not only lead to cement leakage but also increase the risk of cement displacement to a certain extent. Although there is no consensus on the optimal volume of bone cement to inject, Kim et al.[15] believe that the volume of bone cement slightly more than that of the IVC space should be injected to prevent intravertebral instability caused by non-union in percutaneous vertebroplasty for KD. Some scholars[14,31,32] mainly suggest that polymethylmethacrylate cement in vertebroplasty is merely a space-occupying material without mechanical interlocking ability and biocompatibility, meaning that the bone cement and the surrounding bone tissue did not joined, which was another important cause of cement dislodgement. In this study, only two patients in the PKP group had radiographic evidence of bone cement displacement without clinical symptoms, which was suspected to be related to the progression of osteoporosis, anterior cortical defects, and uneven cement distribution.

Some scholars believe that once bone cement displacement occurs, patients often need to undergo open posterior, anterior, or even anterior and posterior revision surgery to remove the displaced bone cement, reconstruct spinal stability, and restore the spinal sequence and fusion.[14,32,33] Hence, several researchers have advocated for the implementation of short or long segmental fixation in conjunction with vertebroplasty to circumvent bone cement displacement. Nonetheless, the drawbacks of this approach, when contrasted with the use of bone cement, include increased surgical trauma, reduced spinal flexibility, more postoperative complications, and high cost.[34,35]

4.3 | Innovation of the hollow pedicle screw system in prevention of bone cement displacement

In this study, a hollow pedicle screw system was used to interlock the bone cement with the surrounding bone tissue, thereby forming a stable and firm complex. This approach aimed to prevent refractory low back pain, spinal instability, spinal cord nerve dysfunction and other problems resulting from bone cement displacement. This innovative concept is in line with Professor Yonezawa,[16,17] who inserted hollow pedicle screws into the cement block through the pedicle to prevent bone cement displacement.[17] In addition, Wang et al.[18] also confirmed the excellent short and medium-term therapeutic effect of a novel bone cement screw system combined with vertebroplasty for KD in preventing bone cement displacement. The difference from Wang's study[18] is that in the present study, bone cement was injected first, and then cannulated pedicle screws were rapidly inserted before the cement set and hardened. This approach can not only effectively utilize the balloon to restore the height of the vertebral body but also ensure the full filling of bone cement in the IVC, enabling the bone cement to fully fuse with the surrounding bone tissue. However, in contrast to Yonezawa's study, the double-thread screw design used in the current study is more suitable for osteoporotic vertebral bodies, and the non-nut screw design reduces damage to muscles and blood vessels.

4.4 | Finite element biomechanical analysis of postoperative vertebral stability in KD models

According to the results, we found that the von Mises stress on T12 in M2 to M6 was significantly decreased compared with M1 (Figure 5C), which indicated the vertebral fracture was significantly improved after surgery, and the vertebral body was more stable, and the occurrence of re-fracture was reduced. Besides, the unilateral injection of bone cement only improves the stiffness of one side of the vertebral body, whereas the other side is still damaged cancellous bone with low stiffness, indicating that the asymmetric distribution of bone cement will lead to stress concentration in the unenhanced side of the vertebral body. Zhang et al.[36] have shown that cement distribution and vertebral stiffness are important factors affecting the stress

balance of the vertebral body for recompression fractures of the vertebral body after PVP. This asymmetric cement distribution may reduce the stiffness of the non-reinforcing side, leading to fracture recurrence.[37]

Does KD increase the risk of adjacent vertebral fracture after PKP or HPS-KP surgery? Peng et al.[38] have shown that increasing the stiffness of bone cement in a finite element model of osteoporosis leads to an increased risk of adjacent vertebral fracture after vertebroplasty. According to the results, the von Mises stress on T11 and L1 of six models increased under flexion and left/right bending, and six models did not differ much under seven loading conditions (Figure 5A,B). Therefore, we contend that the implantation of bone cement and screws following surgery does not confer an increased likelihood of adjacent vertebral fractures. Conversely, it is imperative to instruct patients to avoid excessive spinal flexion activities and trauma. According to the results of the Von Mises stress of the bone cement (Figure 5D), We believe that bilateral surgery with vertebral cement augmentation can achieve better biomechanical stability of the vertebral body compared with unilateral surgery. In addition, this study revealed that stress was concentrated on the hollow pedicle screw in the HPS-KP surgical model. Therefore, special attention should be paid to postoperative mobilization to prevent the risk of screw breakage.

In this study, the cement displacement of M2 and M3 was significantly greater than that of M4, M5 and M6, especially in forward flexion, right bending and left and right rotation, suggesting that cement augmentation alone is more likely to cause cement loosening in flexion and lateral bending. This result is consistent with the biomechanical results of the finite element analysis by wang et al.[13] Therefore, patients should be aware of cement displacement or loosening after PKP alone or unilateral PKP combined with pediculoplasty for KD, especially during flexion, right bending and rotation activities. This may be due to the changes in the center of gravity and stress of the vertebral body during forward flexion and rotation, which is more likely to cause the micromovement of bone cement in the vertebral body. In conclusion, for KD, the hollow pedicle screw system combined with kyphoplasty has better stability and safety than the common simply PKP and PKP combined with pediculoplasty, indicating that this treatment has the best ability to resist bone cement loosening and displacement.

4.5 | Strengths and limitations

Through a comparative 3D finite element biomechanical study, we found that the relative displacement of the cement was the lowest after the application of hollow pedicle screws to lock the cement. However, the finite element analysis only uses the data of one patient, which is lack of representative. Besides, a small sample size may not fully represent the diversity and complexity of the entire patient population, which could potentially lead to results that are not generalized enough. And short follow-up period might not capture the long-term effects and potential complications that could occur over an extended period. Therefore, more biomechanical tests and large-sample prospective studies are needed in the future.

5 | CONCLUSION

HPS-KP shares similar advantages to PKP, including small trauma, effective pain relief, vertebral height restoration, and kyphosis correction. In contrast, HPS-KP offers greater stability than PKP alone or PKP combined with pedicle angioplasty by better balancing stress on the vertebral body and preventing bone cement displacement or loosening. In addition, during postoperative spinal mobilization, flexion, left and right bending, and rotation of the spine should be reduced because these activities may increase the risk of cement displacement.

CONFLICT OF INTEREST STATEMENT
None of the authors has any potential conflict of interest.

ORCID
Shixiao Zhong https://orcid.org/0000-0003-4209-4933

REFERENCES

1. Brower AC, Downey EF Jr. Kummell disease: report of a case with serial radiographs. *Radiology*. 1981;141(2):363-364.
2. Matzaroglou C, Georgiou CS, Panagopoulos A, et al. Kummell's disease: clarifying the mechanisms and patients' inclusion criteria. *Open Orthop J*. 2014;8:288-297.
3. He D, Yu W, Chen Z, Li L, Zhu K, Fan S. Pathogenesis of the intravertebral vacuum of Kummell's disease. *Exp Ther Med*. 2016;12(2):879-882.
4. Li K-C, Wong T-U, Kung F-C, Li A, Hsieh CH. Staging of Kümmell's disease. *J Musculoskelet Res*. 2004;8(1):43-55.
5. Jindal V, Binyala S, Kohli SS. Balloon kyphoplasty versus percutaneous vertebroplasty for osteoporotic vertebral body compression fractures: clinical and radiological outcomes. *Spine J*. 2023;23(4):579-584.
6. Adamska O, Modzelewski K, Stolarczyk A, Kseniuk J. Is Kummell's disease a misdiagnosed and/or an underreported complication of osteoporotic vertebral compression fractures? A pattern of the condition and available treatment modalities. *J Clin Med*. 2021;10(12):2584.
7. Rocha Romero A, Hernandez-Porras BC, Plancarte-Sanchez R, et al. Risk of new fractures in Vertebroplasty for multiple myeloma. A retrospective study. *Pain Med (Malden, Mass)*. 2020;21(11):3018-3023.
8. Zhang J, Fan Y, He X, et al. Is percutaneous kyphoplasty the better choice for minimally invasive treatment of neurologically intact osteoporotic Kummell's disease? A comparison of two minimally invasive procedures. *Int Orthop*. 2018;42(6):1321-1326.
9. Gao X, Du J, Gao L, et al. Risk factors for bone cement displacement after percutaneous vertebral augmentation for osteoporotic vertebral compression fractures. *Front Surg*. 2022;9:947212.

10. Gao X, Du J, Zhang Y, et al. Predictive factors for bone cement displacement following percutaneous vertebral augmentation in Kummell's disease. *J Clin Med.* 2022;11(24):7479.

11. Wang HS, Kim HS, Ju CI, Kim SW. Delayed bone cement displacement following balloon kyphoplasty. *J Korean Neurosurg Soc.* 2008;43(4):212-214.

12. Ohba T, Ebata S, Clinton D, Koyama K, Haro H. Instability of treated vertebrae after balloon kyphoplasty causing paraparesis in osteoporotic vertebral compression fracture: a report of two cases. *Eur Spine J.* 2013;22(Suppl 3):S341-S345.

13. Wang B, Zhan Y, Bai Y, et al. Biomechanical analysis of a novel bone cement bridging screw system for the treatment of Kummell disease: a finite element analysis. *Am J Transl Res.* 2022;14(10):7052-7062.

14. Tsai TT, Chen WJ, Lai PL, et al. Polymethylmethacrylate cement dislodgment following percutaneous vertebroplasty: a case report. *Spine (Phila Pa 1976).* 2003;28(22):E457-E460.

15. Kim JE, Choi SS, Lee MK, Lee DK, Cho SI. Failed percutaneous Vertebroplasty due to insufficient correction of Intravertebral instability in Kummell's disease: a case report. *Pain Pract.* 2017;17(8):1109-1114.

16. Yonezawa Y, Yonezawa N, Kanazawa Y, Yonezawa T, Yonezawa K, Demura S. Revision balloon kyphoplasty and vertebra-pediculoplasty using cannulated screws for osteoporotic vertebral fractures with cement dislodgement following conventional balloon kyphoplasty. *J Neurointerv Surg.* 2022;14(8):844-846.

17. Yonezawa N, Yonezawa Y, Nishimura T, et al. Vertebra-Pediculoplasty: a new approach to treatment of Split-type and delayed-union osteoporotic vertebral fracture with a risk of cement dislodgement. *World Neurosurg.* 2021;155:e55-e63.

18. Wang B, Wang Y, Zhang H, et al. A novel bone cement screw system combined with vertebroplasty for the treatment of Kummell disease with bone deficiency at the vertebral anterior border: a minimum 3-year follow-up study. *Clin Neurol Neurosurg.* 2021;201:106434.

19. Lu J, Ren Z, Liu X, Xu YJ, Liu Q. Osteoporotic fracture guidelines and medical education related to the clinical practices: a Nationwide survey in China. *Orthop Surg.* 2019;11(4):569-577.

20. Polikeit A, Nolte LP, Ferguson SJ. The effect of cement augmentation on the load transfer in an osteoporotic functional spinal unit: finite-element analysis. *Spine (Phila Pa 1976).* 2003;28(10):991-996.

21. Kim HJ, Chun HJ, Kang KT, et al. The biomechanical effect of pedicle screws' insertion angle and position on the superior adjacent segment in 1 segment lumbar fusion. *Spine (Phila Pa 1976).* 2012;37(19):1637-1644.

22. Zhao WT, Qin DP, Zhang XG, Wang ZP, Tong Z. Biomechanical effects of different vertebral heights after augmentation of osteoporotic vertebral compression fracture: a three-dimensional finite element analysis. *J Orthop Surg Res.* 2018;13(1):32.

23. Lu H, Zhang Q, Ding F, Wu Q, Liu R. Finite element analysis of unilateral versus Bipedicular bone-filling mesh container for the Management of Osteoporotic Compression Fractures. *Biomed Res Int.* 2022;2022:6850089.

24. Wilke HJ, Wenger K, Claes L. Testing criteria for spinal implants: recommendations for the standardization of in vitro stability testing of spinal implants. *Eur Spine J.* 1998;7(2):148-154.

25. Panjabi MM, Kifune M, Liu W, Arand M, Vasavada A, Oxland TR. Graded thoracolumbar spinal injuries: development of multidirectional instability. *Eur Spine J.* 1998;7(4):332-339.

26. Wang G, Yang H, Chen K. Osteoporotic vertebral compression fractures with an intravertebral cleft treated by percutaneous balloon kyphoplasty. *J Bone Joint Surg Br.* 2010;92(11):1553-1557.

27. Fan N, Wang T, Wang A, et al. A predictive nomogram for intradiscal cement leakage in percutaneous kyphoplasty for osteoporotic vertebral compression fractures combined with intravertebral cleft. *Front Surg.* 2022;9:1005220.

28. Lin WC, Lee YC, Lee CH, et al. Refractures in cemented vertebrae after percutaneous vertebroplasty: a retrospective analysis. *Eur Spine J.* 2008;17(4):592-599.

29. Heo DH, Chin DK, Yoon YS, Kuh SU. Recollapse of previous vertebral compression fracture after percutaneous vertebroplasty. *Osteoporos Int.* 2009;20(3):473-480.

30. Yu WB, Jiang XB, Liang D, Xu WX, Ye LQ, Wang J. Risk factors and score for recollapse of the augmented vertebrae after percutaneous vertebroplasty in osteoporotic vertebral compression fractures. *Osteoporos Int.* 2019;30(2):423-430.

31. Jeong YH, Lee CJ, Yeon JT, et al. Insufficient penetration of bone cement into the trabecular bone: a potential risk for delayed bone cement displacement after Kyphoplasty? *Reg Anesth Pain Med.* 2016;41(5):616-618.

32. Nagad P, Rawall S, Kundnani V, Mohan K, Patil SS, Nene A. Postvertebroplasty instability. *J Neurosurg Spine.* 2012;16(4):387-393.

33. Zhang C, Wang G, Liu X, Li Y, Sun J. Failed percutaneous kyphoplasty in treatment of Stage 3 Kummell disease: a case report and literature review. *Medicine (Baltimore).* 2017;96(47):e8895.

34. Liu Y, Zhu Y, Li R, Jiang W, Yang H. Comparison between percutaneous Kyphoplasty and posterior fixation combined with Vertebroplasty in the treatment of stage III Kummell's disease without neurological deficit. *Biomed Res Int.* 2022;2022:2193895.

35. Li H-K, Hao D-J, Yang J-S, et al. Percutaneous kyphoplasty versus posterior spinal fixation with vertebroplasty for treatment of Kümmell disease: a case-control study with minimal 2-year follow-up. *Medicine.* 2017;96(51):e9287.

36. Zhang L, Wang Q, Wang L, Shen J, Zhang Q, Sun C. Bone cement distribution in the vertebral body affects chances of recompression after percutaneous vertebroplasty treatment in elderly patients with osteoporotic vertebral compression fractures. *Clin Interv Aging.* 2017;12:431-436.

37. Dai H, Liu Y, Han Q, et al. Biomechanical comparison between unilateral and bilateral percutaneous vertebroplasty for osteoporotic vertebral compression fractures: a finite element analysis. *Front Bioeng Biotechnol.* 2022;10:978917.

38. Peng Y, Du X, Huang L, et al. Optimizing bone cement stiffness for vertebroplasty through biomechanical effects analysis based on patient-specific three-dimensional finite element modeling. *Med Biol Eng Comput.* 2018;56(11):2137-2150.